Nanoscale Advances

COMMUNICATION

View Article Online
View Journal | View Issue

Cite this: *Nanoscale Adv.*, 2019, **1**, 980

Synthesis of stable and phase-adjustable $CsPbBr_3$@Cs_4PbBr_6 nanocrystals *via* novel anion–cation reactions†

Received 19th October 2018
Accepted 23rd December 2018

DOI: 10.1039/c8na00291f

rsc.li/nanoscale-advances

Leimeng Xu, Jianhai Li, Tao Fang, Yongli Zhao, Shichen Yuan, Yuhui Dong and Jizhong Song *

All-inorganic cesium lead halide perovskites have emerged as promising semiconductor materials due to their preeminent performance in lighting, display, light detecting, and laser fields. However, the applications of lead halide perovskites are limited by the dissatisfactory stability owing to their fragile ionic crystal characteristics and highly dynamic surface-coordinated states. The *in situ* diphase structure passivation possessing the same chemical constituents (such as passivating $CsPbBr_3$ with Cs_4PbBr_6) has been proven to be an effective way to improve the stabilities and simultaneously maintain the highly efficient luminescence properties. Herein, for the first time, we report a novel anion–cation reaction method to synthesize the lead halide perovskite NCs with diphase $CsPbBr_3$@Cs_4PbBr_6 structure. Moreover, we have found that the phase transformation between $CsPbBr_3$ and Cs_4PbBr_6 is temperature dependent. Thus, we could control the relative composition of the diphase $CsPbBr_3$@Cs_4PbBr_6 composite by adjusting the temperature. The optimized $CsPbBr_3$@Cs_4PbBr_6 composite NCs achieve highly light emissive performance and stabilities against atmosphere, moisture and heating. Furthermore, we could obtain 135% of the NTSC color gamut through anion exchange. These highly emissive composite NCs with improved stabilities exhibit great potential in future optoelectronic fields.

Introduction

Lead halide perovskites gained increasing attention in light-emitting diodes (LED),[1–8] photodetectors,[9–12] and lasers[13] in recent years due to their ultrahigh photoluminescence quantum yields (PLQYs), good carrier mobility, multicolor electroluminescence, and low-threshold lasing. The high-performance halide perovskite is commonly used in the form of three-dimensional (3D) cubic or monoclinic phase,[14–18] $CsPbX_3$ (X = Cl, Br, I), which is known to be composed of corner-shared PbX_6^{4-} octahedron and filling Cs^+ ions.[14] However, this structure is affected by its fragility against moisture, illumination, and heating for its intrinsic ionic characteristics and easy-lost halide atoms.[19,20] Agglomeration of NCs,[21] polar solvents[22] or even the ultraviolet light[23] can easily degrade the luminescence or damage the structure, which restricts further application in photonics and optoelectronics. To overcome the above-mentioned concerns, a lot of strategies have been designed to improve the stability of perovskite NCs, for example, Sun *et al.* wrapped halide perovskite QDs in a cross-linked silica matrix,[24] Guarnera *et al.* improved the stabilities *via* perovskites coating with Al_2O_3,[25] and some other studies obtained water-resistant $CsPbX_3$ NCs *via* embedding NCs into polymer materials.[26,27] In general, it seems to be an effective strategy that we package the perovskite NCs into tough capsulations to resist the harsh conditions outside. However, the introduced additive may affect the original luminescence of NCs, and also increase the complexity of the process.

Recently, the zero-dimensional (0D) Cs_4PbBr_6, another derived phase of $CsPbBr_3$ NCs,[28–31] could provide *in situ* passivation for $CsPbBr_3$ NCs.[15,32–34] Cs_4PbBr_6 has been reported to be a natural insulator possessing air-stable and robust properties,[29,35,36] which shares the same components with $CsPbBr_3$. In addition, Quan *et al.*[29] has proven that the lattice of Cs_4PbBr_6 matches with that of $CsPbBr_3$ in one direction, which protects a $CsPbBr_3$ NC growing inside a Cs_4PbBr_6 matrix. The $PbBr_6^{4-}$ octahedra of Cs_4PbBr_6 are separated by corner Cs^+ without sharing Br^- with each other, and the individual $PbBr_6^{4-}$ octahedron is not connected to the adjacent octahedron leading to the localized excitons in an isolated octahedron, the so-called 0D perovskites. 0D Cs_4PbBr_6 NCs are generally obtained by adjusting the components or regulating the surface ligands, for instance, the high ratio of Cs/Pb environment was favorable to form Cs_4PbBr_6,[29,37] or directly transforming from $CsPbBr_3$ NCs in a rich Cs^+ condition,[35] and mediating the surface ligands with more oleylamine could stimulate the formation of Cs_4PbBr_6.[38,39] However, there are only few studies reporting the synthesis of component-controllable $CsPbBr_3$@Cs_4PbBr_6 composite NCs.

MIIT Key Laboratory of Advanced Display Materials and Devices, Institute of Optoelectronics and Nanomaterials, School of Materials Science and Engineering, Nanjing University of Science and Technology, Nanjing 210094, China. E-mail: songjizhong@njust.edu.cn

† Electronic supplementary information (ESI) available. See DOI: 10.1039/c8na00291f

Moreover, all these syntheses are based on the re-precipitation method, which is conducted by injecting dimethylformamide (DMF) solution containing CsBr and $PbBr_2$ into the poor solvent. Thus, the production of $CsPbBr_3@Cs_4PbBr_6$ NCs is limited by the low solubility of CsBr in DMF, particularly for the method needing rich-Cs^+ environment. Therefore, exploring a new approach to simultaneously obtain high-yield and phase-adjustable $CsPbBr_3@Cs_4PbBr_6$ NCs is of great importance for industrialization.

Herein, for the first time, we developed a novel anion–cation method to synthesize phase-adjustable $CsPbBr_3@Cs_4PbBr_6$ composite NCs under atmospheric conditions. In this method, an active brominated agent, pyridinium tribromide (PDBr), was used as the source of bromine; however, cesium acetate and lead acetate with higher solubility were used to replace CsBr and $PbBr_2$. Besides being used as the source of bromine, PDBr provided highly Br^--rich conditions for the growth of perovskites to obtain high-quality crystalline structures with few surface defects. Furthermore, we found that the phase transformation between $CsPbBr_3$ and Cs_4PbBr_6 was temperature dependent. Cs_4PbBr_6 NCs were preferred to be formed at lower temperatures, while increasing the temperature gave rise to more $CsPbBr_3$ NCs. Relative proportions of $CsPbBr_3$ and Cs_4PbBr_6 were calculated from the XRD pattern at different temperatures and the corresponding optical properties were discussed. The optimized sample showed strong green PL emission with a full width at half maximum (FWHM) of 19 nm. PL attenuation curves and PL lifetime demonstrate the greatly improved stabilities and efficient trap-passivation of $CsPbBr_3@Cs_4PbBr_6$ NCs compared to naked $CsPbBr_3$ NCs with cubic or monoclinic phase. Furthermore, a wide color gamut of 135% of the NTSC standard was obtained *via* anion exchange. The as-proposed novel anion–cation method paves the way for the mass production of stable and highly emissive perovskite NCs, which have a huge potential application in lightings, displays, and lasers.

Results and discussion

Emissive 3D $CsPbBr_3$ NCs are usually used in the form of cubic and monoclinic phases, whose structures are presented in Fig. 1a and b, respectively. Cubic and monoclinic $CsPbBr_3$ NCs possess similar lattice arrangements, the difference being that the latter has tilting octahedra compared to the former.[40] Cubic and monoclinic $CsPbBr_3$ NCs also exhibit similar optical properties and structural characteristics[16] facing the same stability issue. Well, compared to $CsPbBr_3$ with cubic or monoclinic structure, the octahedra of rhombohedral Cs_4PbX_6 were decoupled completely (Fig. 1c), making it a 0D structure. Thus, Cs_4PbBr_6 NCs have quite different properties,[41,42] such as colorless crystals with wider band gap (3.95 eV)[43] and better environmental tolerance,[29,38] which make it perfect for capsulation.

Cubic NCs are usually synthesized by hot-injection (HI),[17,44] and by injecting oleic cesium precursors into high-temperature solvents containing $PbBr_2$ and ligands under inert environments, as shown in Fig. 2. Monoclinic $CsPbBr_3$ NCs (PDF#18-0346) are widely obtained *via* room-temperature re-precipitation (RP)[16] that is conducted by adding the as-prepared $CsBr/PbBr_2$ precursors into poor solvents (Fig. 2) under atmospheric environment. Previous reports[30,39] have demonstrated that $CsPbBr_3$ could be converted into Cs_4PbBr_6, and Cs_4PbBr_6 could also be converted into $CsPbBr_3$ with excess $PbBr_2$, proving the feasibility of passivating $CsPbBr_3$ with Cs_4PbBr_6. Now, Cs_4PbBr_6 NCs are generally obtained *via* modified RP by using excess Cs^+ (ref. 35 and 45) or ligand-mediating method.[38,39] Herein, we put forward a novel anion–cation reaction method without forming $PbBr_6^{4-}$ octahedral precursors in advance to prepare perovskite NCs. The schematic of the anion–cation reaction is shown in Fig. 2, wherein an active brominated agent, pyridinium tribromide (PDBr), was introduced to act as a halogen source. In a typical synthesis, the *N*,*N*-dimethyl formamide (DMF) solutions of $Pb(Ac)_2$ and Cs(Ac) were added to toluene containing organic ligands and then, bromine-rich pyridinium tribromide was swiftly added at an appropriate temperature to form perovskite NCs. The adequate Br^- of PDBr provides a Br^--rich condition for perovskites to obtain high-quality NCs with less bromine vacancies.[46]

Through this novel anion–cation reaction method, a typical solution sample of $CsPbBr_3@Cs_4PbBr_6$ NCs was obtained (shown in Fig. 3a), which exhibited bright photoluminescence

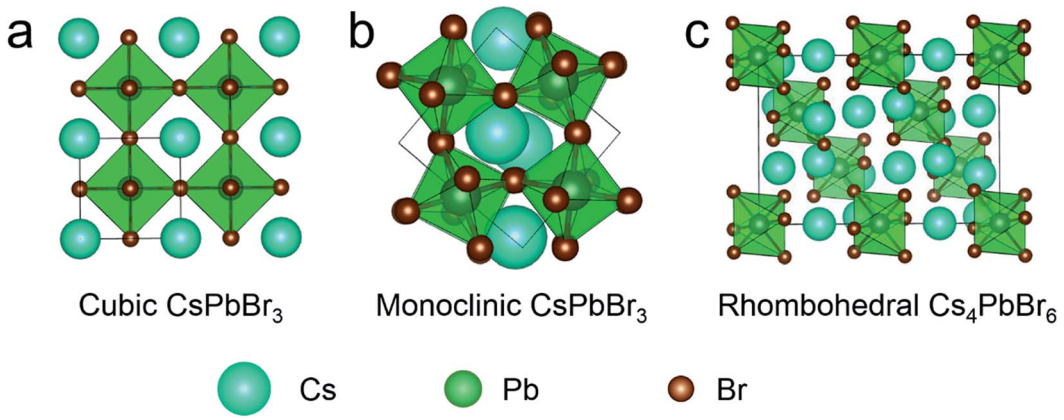

Fig. 1 Simulated crystal structure of (a) cubic $CsPbBr_3$, (b) monoclinic $CsPbBr_3$ and (c) rhombohedral Cs_4PbBr_6.

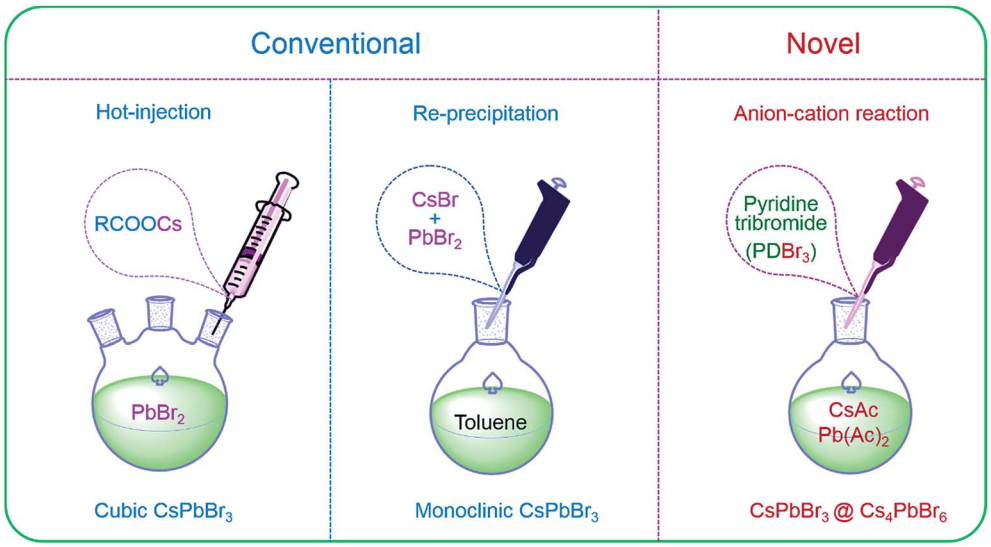

Fig. 2 Schematic of the hot-injection, re-precipitation and anion–cation reactions for cubic $CsPbBr_3$, monoclinic $CsPbBr_3$ and $CsPbBr_3$@-Cs_4PbBr_6 NCs.

(PL) at 513 nm with a full width at half maximum (FWHM) of 19 nm (Fig. 3b). The dazzling green emission of $CsPbBr_3$@-Cs_4PbBr_6 came from $CsPbBr_3$ NCs because Cs_4PbBr_6 NCs owning colorless crystals with wide band gap. Compared to the greatly degenerating PLQY of solid $CsPbBr_3$ NCs,[1,29] the powder of $CsPbBr_3$@Cs_4PbBr_6 NCs (inset photographs in Fig. 3b) could maintain 51% PL QY. The photoluminescence stabilities of different phases will be discussed later. The $CsPbBr_3$@Cs_4PbBr_6 NCs exhibited the rhombus morphology of rhombohedral Cs_4-$PbBr_6$ matrix with an average size of 60 nm (Fig. 3c). From the SEM and TEM images in Fig. 3c and d, the morphology of the NCs exhibited consistent and uniform rhombus without cubes; however, the XRD pattern in Fig. 3e reveals the coexistence of $CsPbBr_3$ and Cs_4PbBr_6. These observations indicate that the $CsPbBr_3$ NCs grew inside the Cs_4PbBr_6 matrix, which is simplified in the inset diagrammatic figure in Fig. 3c. To demonstrate the capacity of this anion–cation method for volume production, we expanded the scale by 25-fold to 500 mL. The photograph of the expanded manufacture is presented in the inset of Fig. 4a. The PL peak of the obtained NCs is at 513 nm (Fig. 4a), possessing the same peak position with the small scale. The SEM image (Fig. 4b) of the large-scale manufacture also shows the homogeneous rhombus crystals without small particle impurities in a wide range. These results demonstrate the great potential of the anion–cation method for industrialization.

Previous works[30,35,41,47] have reported that high ratio of Cs^+/Pb^{2+} over 1 is beneficial for the formation of Cs_4PbBr_6, and the adjustment of the ratio can yield different proportions of $CsPbBr_3$@Cs_4PbBr_6 compounds. At the same time, some other reports[39] also demonstrated that surface ligands can regulate the phase transformation between $CsPbBr_3$ and Cs_4PbBr_6. In this system, we found that temperature also played a vital role in the formation of phase structure. The proportion of $CsPbBr_3$ and Cs_4PbBr_6 were regulated by controlling the temperature from 25 °C to 80 °C (Fig. 5) with a Cs^+/Pb^{2+} ratio of 1. The bottom of the abscissa in Fig. 5e shows the standard peaks of dominant rhombohedral phase (PDF#73-2478), while the opposite shows the standard peaks of cubic phase (PDF#54-0752). At a temperature of 25 °C, the XRD pattern (Fig. 5e) shows that the main peaks all from the rhombohedral and cubic phases are unconspicuous. The corresponding SEM image in Fig. 5a also presents consistent morphological features. With the temperature increasing to 40 °C and 60 °C, new peaks at 15.1°, 21.5°, 30.6°, 37.8°, and 46.7° enhanced gradually, which corresponds to the (100), (110), (200), (211), and (300) lattice planes of cubic $CsPbBr_3$ NCs. Simultaneously, the peak intensities of Cs_4PbBr_6 become weaker, while view of SEM (Fig. 5b and c) images maintains a uniform rhombic shape without impurities at 40 °C and 60 °C, which demonstrate the effective embedding of cubic $CsPbBr_3$ NCs in Cs_4PbBr_6. We calculate the relative content of $CsPbBr_3$ and Cs_4PbBr_6 phases by the area method. Only a tiny amount (2.4%) of cubic phase could be obtained at room temperature and higher proportion of $CsPbBr_3$ (15.4% and 44.5%, respectively) came into being with the increase in temperature. The productions of 44.5% $CsPbBr_3$ under 60 °C almost resulted in the diamond shape without cubes, as shown in Fig. 5c, which confirmed the formation of $CsPbBr_3$@Cs_4-$PbBr_6$ composite NCs. While with the temperature increasing to 80 °C, $CsPbBr_3$ NCs began to nucleate and grow separated from Cs_4PbBr_6 matrix into independent bulk alone, as seen from the typical cuboidal NC marked in Fig. 5d. In addition, the XRD pattern in Fig. 5e reveals that only a fraction of Cs_4PbBr_6 existed in the composites. When the temperature was higher than 100 °C, the cubic phase accounted for the vast majority (more than 90%). The relation between the proportions of these two phases and the temperature is listed in Table 1. Cs_4PbBr_6 NCs were preferred to form at lower temperature, while higher temperature conditions were more conductive to the formation of cubic phase, and higher temperature also created a more

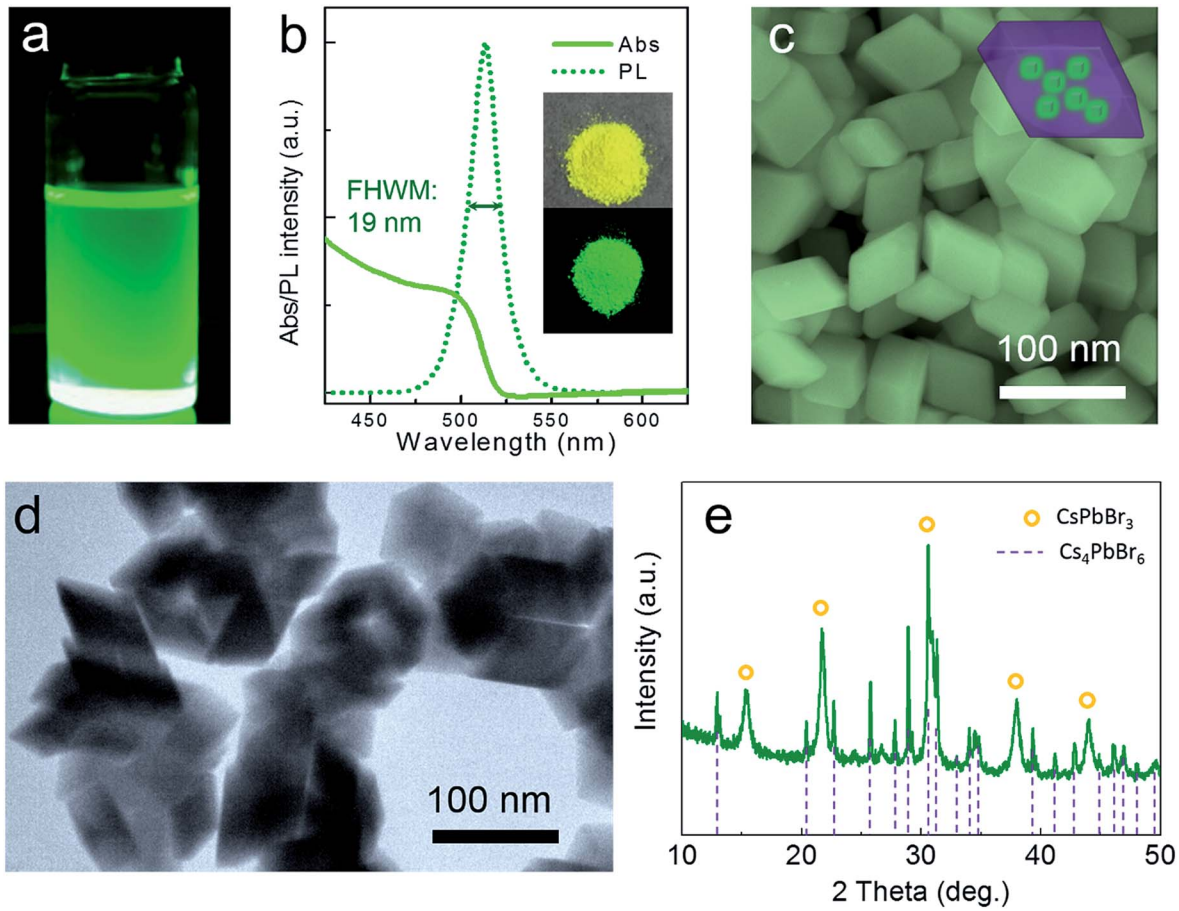

Fig. 3 Typical $CsPbBr_3$@Cs_4PbBr_6 sample: (a) toluene dispersion under UV light. (b) PL and absorption spectrum. Inset: photographs of powder sample under day light and UV light, respectively. (c) SEM image of typical $CsPbBr_3$@Cs_4PbBr_6. Inset: schematics of the microstructure. (d) TEM image of the typical $CsPbBr_3$@Cs_4PbBr_6. (e) XRD pattern of the typical $CsPbBr_3$@Cs_4PbBr_6.

violent reactivity, thereby leading to independent nucleation and growth of $CsPbBr_3$ NCs.

Temperature could not only adjust the phase composition but also influence the optical properties. Fig. 6a exhibits solution samples synthesized at different temperatures and their corresponding PL spectra. Blue emission (480 nm) is observed when reaction temperature is 20 °C, which could be explained by the dimensionality reduction of embedded $CsPbBr_3$ NCs resulted from lower temperature.[48,49] With the increase in temperature, the spectra reveal a slight redshift due to the aggregation and size of $CsPbBr_3$ NCs with the increasing proportion. The broader FWHM at 20 °C and 40 °C maybe the

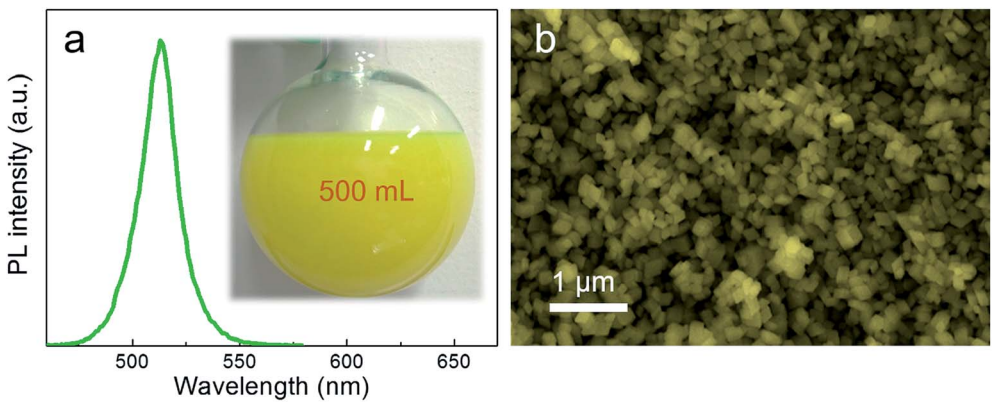

Fig. 4 (a) PL spectrum of large-yield $CsPbBr_3$@Cs_4PbBr_6 NCs, inset is the photograph of large-yield reaction product. (b) Large-scale SEM image of high yields of $CsPbBr_3$@Cs_4PbBr_6 NCs.

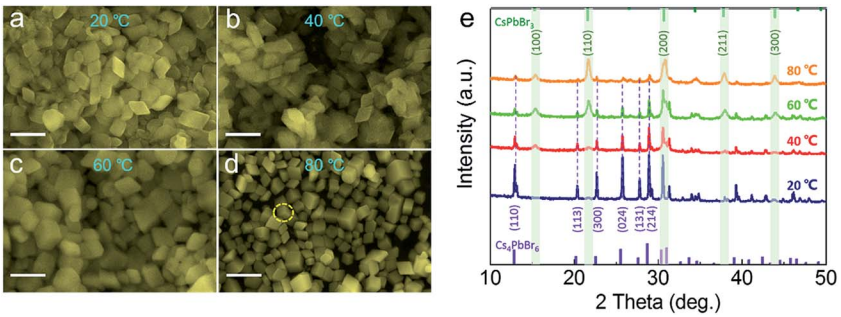

Fig. 5 SEM images of products prepared at different temperatures: (a) 20 °C, (b) 40 °C, (c) 60 °C and (d) 80 °C. (e) The corresponding XRD patterns of products prepared at different temperatures.

Table 1 The corresponding proportion of $CsPbBr_3$ controlled by different temperatures

T/°C	20	40	60	80
Ratio/$CsPbBr_3$	2.4%	15.4%	44.5%	80.5%
Ratio/Cs_4PbBr_6	97.6%	84.6%	55.5%	19.5%

Table 2 PL lifetime parameters of $CsPbBr_3$@Cs_4PbBr_6 NCs prepared at different temperatures

T/°C	20	40	60	80
τ_1/ns	6.77	5.83	4.5	2.71
τ_2/ns	22.1	28.36	18.6	14.3
τ_{aver}/ns	23.1	22.3	17.7	15.6

result of uneven size of dysgonic $CsPbBr_3$ NCs. The absorption spectra (Fig. S1†) also exhibited the same trend. PLQY gradually improved with the increasing proportion of $CsPbBr_3$ NCs in the system as shown in Fig. 6b. However, owing to the dissociative $CsPbBr_3$ NCs, the PL lifetime of composites obtained at 80 °C was sharply decreased (Fig. 6c). Longer lifetime was detected as the Cs_4PbBr_6 matrix increased, which is consistent with the previous reports. Detailed parameters of the PL lifetime are listed in Table 2. $CsPbBr_3$@Cs_4PbBr_6 synthesized at 60 °C (with 44.5% $CsPbBr_3$) shows the best excitons combination performance, which was chosen to conduct the following stability tests.

We compared $CsPbBr_3$@Cs_4PbBr_6 composite NCs with monoclinic $CsPbBr_3$ and cubic $CsPbBr_3$ NCs separately to verify its improved stabilities. The cubic $CsPbBr_3$ NCs were synthesized by traditional hot-injection, whereas the monoclinic $CsPbBr_3$ NCs were synthesized by re-precipitation (see ESI†). For better comparison tests, we mixed the NCs ($CsPbBr_3$@Cs_4PbBr_6, monoclinic $CsPbBr_3$ and cubic $CsPbBr_3$) with polydimethylsiloxane (PDMS) to form films, respectively, as shown in the inset photographs of Fig. 7a. It could be seen that $CsPbBr_3$@Cs_4PbBr_6 NCs maintained the best photoluminescence, while severe quenching occurred on both cubic and monoclinic $CsPbBr_3$ NCs. The certain arrangement of $CsPbBr_3$ NCs in Cs_4PbBr_6 made $CsPbBr_3$@Cs_4PbBr_6 NCs have a narrower FWHM compared to HI cubic $CsPbBr_3$ NCs. The slight differences in PL spectra (Fig. 7a) were probably caused by the size effect. The PL decay curves of the three are presented in Fig. 7b. The average lifetime of cubic and monoclinic $CsPbBr_3$ were 5.7 ns and 5.5 ns, while an increasing radiative lifetime of 17.7 ns was evidenced in $CsPbBr_3$@Cs_4PbBr_6 compounds (Table 3). In order to further prove the improving stability of $CsPbBr_3$@Cs_4PbBr_6 NCs, the storage stability test and thermal stability test were designed based on the luminescence degradation. Fig. 7c shows the PL intensity decays of

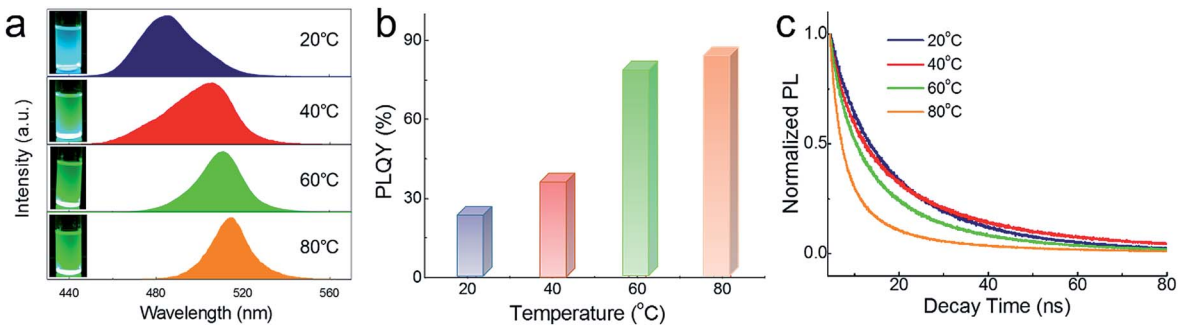

Fig. 6 (a) PL spectra of $CsPbBr_3$@Cs_4PbBr_6 NCs prepared at 20 °C, 40 °C, 60 °C and 80 °C, respectively. Inset: the corresponding photographs of the $CsPbBr_3$@Cs_4PbBr_6 NC samples prepared at different temperatures. (b) PLQY of $CsPbBr_3$@Cs_4PbBr_6 NCs synthesized at 20 °C, 40 °C, 60 °C and 80 °C. (c) PL decay of $CsPbBr_3$@Cs_4PbBr_6 NCs synthesized at 20 °C, 40 °C, 60 °C and 80 °C.

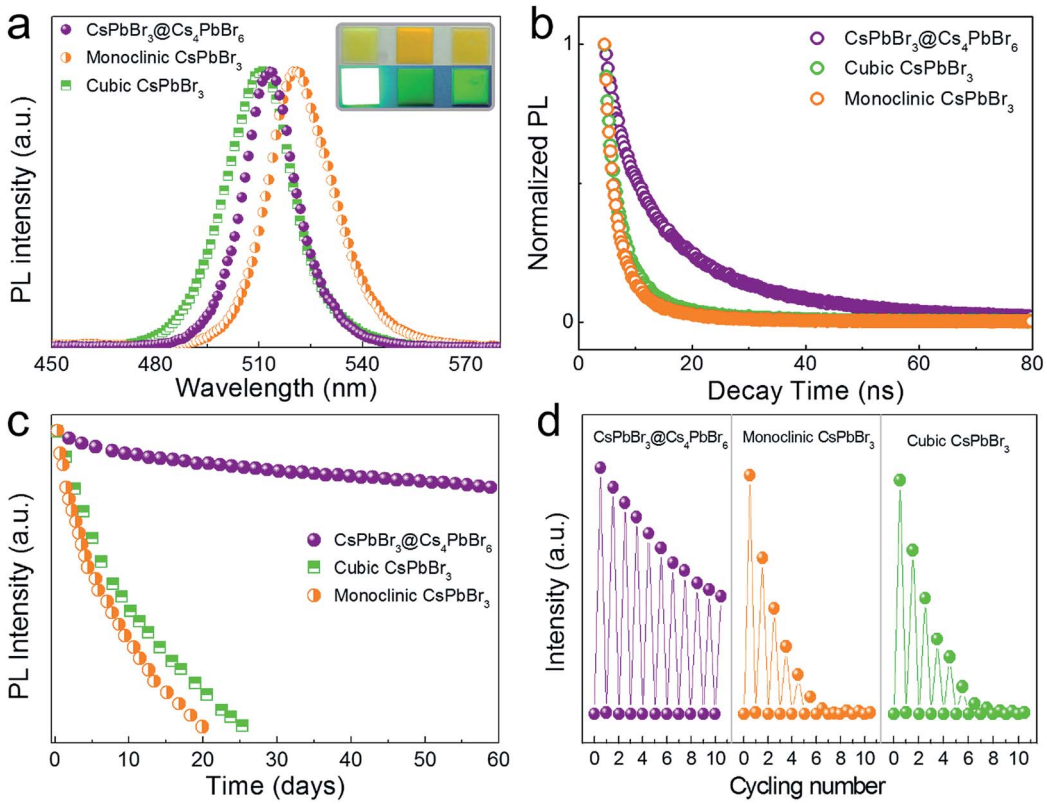

Fig. 7 (a) PL spectra and inset photographs (from left to right) of $CsPbBr_3@Cs_4PbBr_6$, monoclinic $CsPbBr_3$ and cubic $CsPbBr_3$ films (mixing with PDMS). (b) PL decays of $CsPbBr_3@Cs_4PbBr_6$, monoclinic $CsPbBr_3$ and cubic $CsPbBr_3$ films. (c) Storage stability tests of $CsPbBr_3@Cs_4PbBr_6$, monoclinic $CsPbBr_3$ and cubic $CsPbBr_3$ under ambient conditions with RH 50% for two months. (d) Thermal-stability tests of $CsPbBr_3@Cs_4PbBr_6$, monoclinic $CsPbBr_3$ and cubic $CsPbBr_3$ heated from RT to 150 °C for ten cycles under ambient conditions.

Table 3 PL lifetime parameters of $CsPbBr_3@Cs_4PbBr_6$ NCs, cubic $CsPbBr_3$ NCs and monoclinic $CsPbBr_3$ NCs, respectively

T/°C	$CsPbBr_3@Cs_4PbBr_6$	Cubic $CsPbBr_3$	Monoclinic $CsPbBr_3$
τ_1/ns	4.5	1.83	1.62
τ_2/ns	18.6	7.37	6.33
τ_{aver}/ns	17.7	5.7	5.48

the three films shown in Fig. 7a under ambient storage conditions with RH 50% for two months. The $CsPbBr_3@Cs_4PbBr_6$ film showed a decrease of 19%, while cubic and monoclinic $CsPbBr_3$ films completely lost their emission within one month. The thermal cycling tests (Fig. 7d) were performed from room temperature to 150 °C with RH 50% under ambient conditions. After 10 cycles, $CsPbBr_3@Cs_4PbBr_6$ remained approximately half of the original PL intensity, whereas the cubic $CsPbBr_3$ without Cs_4PbBr_6 passivation degenerated sharply to baseline only for 6 cycles, and monoclinic $CsPbBr_3$ was even worse. In conclusion, $CsPbBr_3@Cs_4PbBr_6$ NCs exhibited improved stability, indicating the effective protection of Cs_4PbBr_6, and this new method will take perovskite NCs towards practical applications in optical and photoelectric fields.

We could obtain blue- and red-emitting NCs based on green emitting $CsPbBr_3@Cs_4PbBr_6$ NCs *via* anion exchange. Didodecyldimethylammonium chloride (DDA-Cl) was used for the (Cl/Br)-based blue NCs, and oleylamine iodine (OAm-I) was chosen for red NCs. The schematic of the anion exchange is presented in Fig. 8a, and the amount of DDA-Cl and OAm-I affected the light emissive colors. The photograph of the obtained solution samples under daylight and ultraviolet light is presented in Fig. 8a. Fig. 8b exhibits the corresponding PL spectra, blue to 437 nm and red to 630 nm. We mark the commission Internationale del'Eclairage (CIE) of our spectra using solid line in Fig. 8b; the dashed line area is NTSC standard. It could be seen that our CIE encompasses 135% of the NTSC standard.

A backlit LED was assembled using the as-prepared $CsPbBr_3@Cs_4PbBr_6$ powder and a 450 nm blue chip as shown in the insert photograph of Fig. 9a, which showed the EL spectra of the LED under increasing current (2–12 mA). The EL intensity gradually increased with the increase in current. We continuously light the LED for 10 days in ambient environment (under 8 mA), and no obvious attenuation was observed on the LED (Fig. 9b). All these results imply the huge applicable value of $CsPbBr_3@Cs_4PbBr_6$ NCs in display and lighting fields.

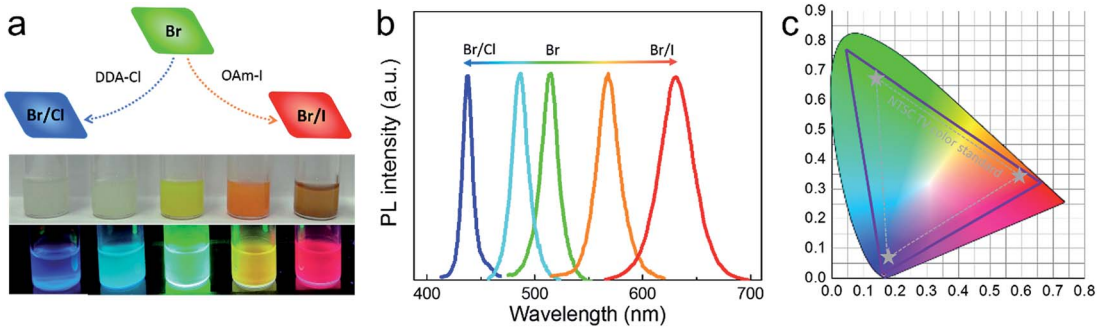

Fig. 8 (a) Schematic of anion exchange with DDACl and OAmI for blue and red spectra, and the corresponding solution samples after anion exchange (blue to red from left to right). (b) The PL spectra of typical samples from blue to red. (c) Solid line area is CIE coordinates of NCs after anion exchange, and the dashed area is the standard NTSC TV color.

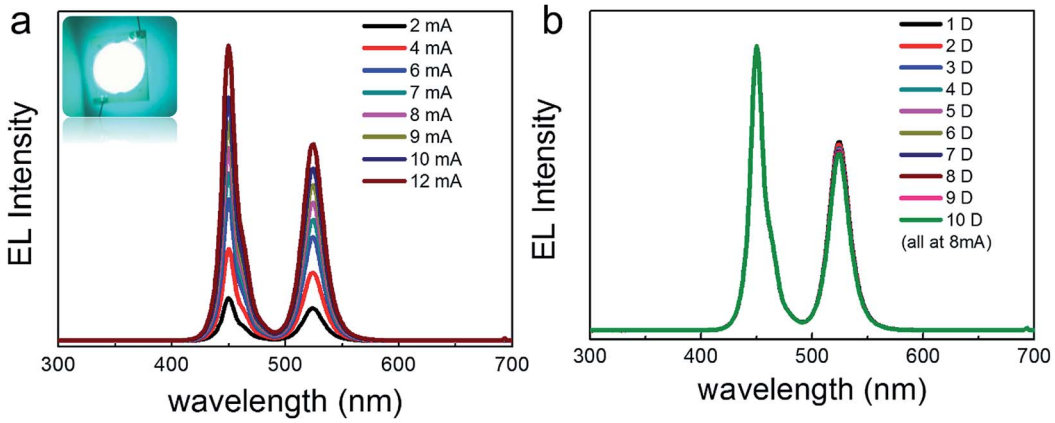

Fig. 9 (a) EL spectra of the $CsPbBr_3$@Cs_4PbBr_6 NC powder-based backlit LED under different currents; inset is the photograph of the backlit LED. (b) EL spectra of the $CsPbBr_3$@Cs_4PbBr_6-based backlit LED lighted for 10 days under ambient conditions.

Conclusion

In summary, a novel anion–cation reaction method was proposed to synthesize the highly emissive $CsPbBr_3$ NCs embedded in the air-stable and crystalline Cs_4PbBr_6 matrix. In this method, temperature was used to adjust the relative proportions of $CsPbBr_3$ and Cs_4PbBr_6. Besides narrower FWHM and higher PLQY, the as-prepared $CsPbBr_3$@Cs_4PbBr_6 compound possessed higher optical stability resisting moist ambient condition and heating. The contrast experiments of storage and thermal stability were designed to compare $CsPbBr_3$@Cs_4PbBr_6 with conventional cubic $CsPbBr_3$ and monoclinic $CsPbBr_3$. Furthermore, the mixed halogen perovskite compound with wide color gamut could be obtained *via* simple anion exchange. In conclusion, the compound of $CsPbX_3$@Cs_4PbX_6 provided a new passage to improve the stability of perovskite, which would be of great significance in lightings, displays, backlights, and other optoelectronic applications.

Experiment section

Synthesis of $CsPbBr_3$@Cs_4PbBr_6 nanocrystals

The anion–cation reaction procedure of Cs_4PbBr_6@$CsPbBr_3$ was conducted by adding the brominating agent into the precursor solution with the presence of cesium ion and lead ion. Typically, the Cs and Pb precursors were formed by dissolving 0.1 mmol cesium acetate and 0.1 mmol lead acetate into 1 mL *N*,*N*-dimethyl formamide (DMF), and the brominating agent was prepared by dissolving PDBr into DMF at 0.3 mol L^{-1} 1 mL PDBr/DMF bromide solution was added into 20 mL toluene with 0.5 mL oleyl amine (OAm), 0.5 mL oleic acid (OA) and 1 mL (Cs, Pb)/DMF precursor under atmospheric conditions; the reaction solution was further stirred for 10 min.

Purification of Cs_4PbBr_6@$CsPbBr_3$ nanocrystals

The as-prepared Cs_4PbBr_6@$CsPbBr_3$ nanocrystals were collected by adding 20 mL acetonitrile and 10 mL toluene into the original solution, and then centrifuging at 8000 rpm for 3 min. The liquid sample was obtained by dispersing the precipitate into 5 mL toluene, and the powder sample was obtained by vacuum drying.

Anion exchange reactions

Different amounts of OAm-I dispersed in toluene (0.1 mol L^{-1}) were dropped into 1 mL as-obtained Cs_4PbBr_6@$CsPbBr_3$ NC solution for red PL emission, while different amounts of DDA-Cl were added for blue emission. The concrete proposal is listed in Table S2.†

Characterization

Powder X-ray diffraction (XRD) patterns were recorded using a Bruker D8 Advance X-ray Diffractometer at 40 kV and 40 mA using Cu Kα radiation ($\lambda = 1.5406$ Å). The morphologies were investigated using the JEOL JSM-7800F field emission scanning electron microscope (FESEM), and the JEM-2100F and JEM-ARM200F transmission electron microscope (TEM) instruments. PL spectra were recorded using an FLS920P fluorescence spectrometer (Edinburgh Instruments) equipped with a photomultiplier in a thermoelectrically cooled housing (R928P, Hamamatsu) with a 450 W xenon arc lamp used as the excitation source for steady-state spectra. The absolute PL quantum yields were detected using a fluorescence spectrometer with an integrated sphere (Hamamatsu Photonics). The photo-stability measurements were analyzed in a temperature and humidity chamber (25 °C, RH 50%) using a 454 nm LED light (21 mW cm^{-2}) provided by Ocean Optics LS-450.

Conflicts of interest

There are no conflicts to declare.

Acknowledgements

This work was financially supported by NSFC (61604074, 51572128, 51672132, 61725402), the National Key Research and Development Program of China (2016YFB0401701, 2017YFA0305500), the Natural Science Foundation of Jiangsu Province (BK20160827, BK20180020), China Postdoctoral Science Foundation (2016M590455), the Fundamental Research Funds for the Central Universities (No. 30917011202, 30915012205, 30916015106), and PAPD of Jiangsu Higher Education Institutions.

References

1 J. Song, J. Li, X. Li, L. Xu, Y. Dong and H. Zeng, *Adv. Mater.*, 2015, **27**, 7162.
2 J. Song, J. Li, L. Xu, J. Li, F. Zhang, B. Han, Q. Shan and H. Zeng, *Adv. Mater.*, 2018, **30**, 1800764.
3 B. Han, B. Cai, Q. Shan, J. Song, J. Li, F. Zhang, J. Chen, T. Fang, Q. Ji, X. Xu and H. Zeng, *Adv. Funct. Mater.*, 2018, 1804285.
4 Q. Shan, J. Li, J. Song, Y. Zou, L. Xu, J. Xue, Y. Dong, C. Huo, J. Chen, B. Han and H. Zeng, *J. Mater. Chem. C*, 2017, **5**, 4565.
5 J. Song, T. Fang, J. Li, L. Xu, F. Zhang, B. Han, Q. Shan and H. Zeng, *Adv. Mater.*, 2018, **0**, 1805409.
6 F. Zhang, J. Song, B. Han, T. Fang, J. Li and H. Zeng, *Small Methods*, 2018, **2**, 1700382.
7 Y. Wei, Z. Cheng and J. Lin, *Chem. Soc. Rev.*, 2019, **48**, 310.
8 Q. Shan, J. Song, Y. Zou, J. Li, L. Xu, J. Xue, Y. Dong, B. Han, J. Chen and H. Zeng, *Small*, 2017, **13**, 1701770.
9 J. Song, L. Xu, J. Li, J. Xue, Y. Dong, X. Li and H. Zeng, *Adv. Mater.*, 2016, **28**, 4861.
10 S. Zhuo, J. Zhang, Y. Shi, Y. Huang and B. Zhang, *Angew. Chem., Int. Ed.*, 2015, **54**, 5693.
11 J. Xue, Z. Zhu, X. Xu, Y. Gu, S. Wang, L. Xu, Y. Zou, J. Song, H. Zeng and Q. Chen, *Nano Lett.*, 2018, **12**, 7628.
12 Y. Dong, Y. Gu, Y. Zou, J. Song, L. Xu, J. Li, J. Xue, X. Li and H. Zeng, *Small*, 2016, **12**, 5622.
13 H. Zhu, Y. Fu, F. Meng, X. Wu, Z. Gong, Q. Ding, M. V. Gustafsson, M. T. Trinh, S. Jin and X. Zhu, *Nat. Mater.*, 2015, **14**, 636.
14 A. Swarnkar, R. Chulliyil, V. K. Ravi, M. Irfanullah, A. Chowdhury and A. Nag, *Angew. Chem.*, 2015, **127**, 15644.
15 F. Palazon, C. Urso, L. De Trizio, Q. Akkerman, S. Marras, F. Locardi, I. Nelli, M. Ferretti, M. Prato and L. Manna, *ACS Energy Lett.*, 2017, **2**, 2445.
16 X. Li, Y. Wu, S. Zhang, B. Cai, Y. Gu, J. Song and H. Zeng, *Adv. Funct. Mater.*, 2016, **26**, 2435.
17 L. Protesescu, S. Yakunin, M. I. Bodnarchuk, F. Krieg, R. Caputo, C. H. Hendon, R. X. Yang, A. Walsh and M. V. Kovalenko, *Nano Lett.*, 2015, **15**, 3692.
18 Z. C. a. J. Lin, *CrystEngComm*, 2010, **12**, 2646.
19 B. Kang and K. Biswas, *J. Phys. Chem. Lett.*, 2018, **9**, 830.
20 S. Seth and A. Samanta, *J. Phys. Chem. Lett.*, 2017, **8**, 4461.
21 Y. Kim, E. Yassitepe, O. Voznyy, R. Comin, G. Walters, X. Gong, P. Kanjanaboos, A. F. Nogueira and E. H. Sargent, *ACS Appl. Mater. Interfaces*, 2015, **7**, 25007.
22 J. Li, L. Xu, T. Wang, J. Song, J. Chen, J. Xue, Y. Dong, B. Cai, Q. Shan and B. Han, *Adv. Mater.*, 2017, **29**, 1603885.
23 L. Xu, J. Chen, J. Song, J. Li, J. Xue, Y. Dong, B. Cai, Q. Shan, B. Han and H. Zeng, *ACS Appl. Mater. Interfaces*, 2017, **31**, 26556.
24 C. Sun, Y. Zhang, C. Ruan, C. Yin, X. Wang, Y. Wang and W. W. Yu, *Adv. Mater.*, 2016, **28**, 10088.
25 S. Guarnera, A. Abate, W. Zhang, J. M. Foster, G. Richardson, A. Petrozza and H. J. Snaith, *J. Phys. Chem. Lett.*, 2015, **6**, 432.
26 H. Huang, B. Chen, Z. Wang, T. F. Hung, A. S. Susha, H. Zhong and A. L. Rogach, *Chem. Sci.*, 2016, **7**, 5699.
27 Q. Zhou, Z. Bai, W. g. Lu, Y. Wang, B. Zou and H. Zhong, *Adv. Mater.*, 2016, **28**, 9163.
28 K. H. Wang, L. Wu, L. Li, H. B. Yao, H. S. Qian and S. H. Yu, *Angew. Chem., Int. Ed.*, 2016, **55**, 8328.
29 L. N. Quan, R. Quintero-Bermudez, O. Voznyy, G. Walters, A. Jain, J. Z. Fan, X. Zheng, Z. Yang and E. H. Sargent, *Adv. Mater.*, 2017, **29**, 1605945.
30 Q. A. Akkerman, S. Park, E. Radicchi, F. Nunzi, E. Mosconi, F. De Angelis, R. Brescia, P. Rastogi, M. Prato and L. Manna, *Nano Lett.*, 2017, **17**, 1924.
31 X. Zhang, B. Xu, J. Zhang, Y. Gao, Y. Zheng, K. Wang and X. W. Sun, *Adv. Funct. Mater.*, 2016, **26**, 4595.
32 X. Chen, F. Zhang, Y. Ge, L. Shi, S. Huang, J. Tang, Z. Lv, L. Zhang, B. Zou and H. Zhong, *Adv. Funct. Mater.*, 2018, **28**, 1706567.
33 Y. Wang, D. Yu, Z. Wang, X. Li, X. Chen, V. Nalla, H. Zeng and H. Sun, *Small*, 2017, **13**, 1701587.
34 W. H. Junwei Xu, P. Li, D. R. Onken, C. Dun, Y. Guo, C. L. Kamil, B. Ucer, H. Wang, S. M. Geyer, R. T. Williams and a. D. L. Carroll, *Adv. Mater.*, 2017, **29**, 1703703.
35 L. Wu, H. Hu, Y. Xu, S. Jiang, M. Chen, Q. Zhong, D. Yang, Q. Liu, Y. Zhao, B. Sun, Q. Zhang and Y. Yin, *Nano Lett.*, 2017, **17**, 5799.

36 Y. Zhang, M. I. Saidaminov, I. Dursun, H. Yang, B. Murali, E. Alarousu, E. Yengel, B. A. Alshankiti, O. M. Bakr and O. F. Mohammed, *J. Phys. Chem. Lett.*, 2017, **8**, 961.
37 W. H. Junwei Xu, P. Li, D. R. Onken, C. Dun, Y. Guo, K. B. Ucer, C. Lu, H. Wang, S. M. Geyer, R. T. Williams and D. L. Carroll, *Adv. Mater.*, 2017, 1703703.
38 X. Chen, D. Chen, J. Li, G. Fang, H. Sheng and J. Zhong, *Dalton Trans.*, 2018, **47**, 5670.
39 Z. Liu, Y. Bekenstein, X. Ye, S. C. Nguyen, J. Swabeck, D. Zhang, S. T. Lee, P. Yang, W. Ma and A. P. Alivisatos, *J. Am. Chem. Soc.*, 2017, **139**, 5309.
40 I. Y. Zaitseva, I. Kovaleva and V. Fedorov, *Russ. J. Inorg. Chem.*, 2006, **51**, 619.
41 S. Kondo, K. Amaya and T. Saito, *J. Phys.: Condens. Matter*, 2002, **14**, 2093.
42 S. Kondo, A. Masaki, T. Saito and H. Asada, *Solid State Commun.*, 2002, **124**, 211.
43 M. Nikl, E. Mihokova, K. Nitsch, F. Somma, C. Giampaolo, G. Pazzi, P. Fabeni and S. Zazubovich, *Chem. Phys. Lett.*, 1999, **306**, 280.
44 G. G. Huang, C. L. Wang, S. H. Xu, S. F. Zong, J. Lu, Z. Y. Wang, C. G. Lu and Y. P. Cui, *Adv. Mater.*, 2017, **29**, 1700095.
45 C. Weerd, J. Lin, L. Gomez, Y. Fujiwara, K. Suenaga and T. Gregorkiewicz, *J. Phys. Chem. C Nanomater. Interfaces*, 2017, **121**, 19490.
46 J. Pan, L. N. Quan, Y. Zhao, W. Peng, B. Murali, S. P. Sarmah, M. Yuan, L. Sinatra, N. M. Alyami and J. Liu, *Adv. Mater.*, 2016, **28**, 8718.
47 G. Tong, H. Li, Z. Zhu, Y. Zhang, L. Yu, J. Xu and Y. Jiang, *J. Phys. Chem. Lett.*, 2018, **9**, 1592.
48 Y. Bekenstein, B. A. Koscher, S. W. Eaton, P. Yang and A. P. Alivisatos, *J. Am. Chem. Soc.*, 2015, **137**, 16008.
49 H. Huang, A. S. Susha, S. V. Kershaw, T. F. Hung and A. L. Rogach, *Adv. Sci.*, 2015, **2**, 1500194.